Journal of Computational Physics **177,** 156–175 (2002)
doi:10.1006/jcph.2002.7008, available online at http://www.idealibrary.com on IDEAL®

On the Construction of Kinetic Schemes

Taku Ohwada

Department of Aeronautics and Astronautics, Graduate School of Engineering, Kyoto University, Kyoto 606-8501, Japan
E-mail: ohwada@kuaero.kyoto-u.ac.jp

Received July 3, 2001; revised January 8, 2002

A general method for the construction of kinetic schemes of evolutionary equations is illustrated with the simple example of the linear advection equation, where the role of the collision effect is clarified theoretically and numerically. The application to the compressible Euler equation and Navier–Stokes equation is explained. The theoretical backgrounds of the existing kinetic schemes, such as the Pullin scheme for the Euler equation and Chou–Baganoff scheme and modified Prendergast–Xu scheme for the Navier–Stokes equation, are unified and their intrinsic errors are revealed.

Key Words: kinetic scheme; Boltzmann equation; Navier–Stokes equation; Euler equation; Chapman–Enskog expansion.

1. INTRODUCTION

The relation between the gasdynamic equation and its kinetic method is indirect. For example, while the Godunov method solves the Riemann problem of the Euler equation to evaluate the numerical flux, the kinetic flux vector splitting method for a gasdynamic equation such as the Pullin scheme [14] employs the solution of the collisionless Boltzmann equation. Since the Euler equation and Navier–Stokes equation are derived from the Boltzmann equation by the Chapman–Enskog expansion, one may expect an increase in the accuracy of kinetic schemes for these gasdynamic equations by the employment of the Boltzmann equation instead of the collisionless equation. The conclusion of this plausible scenario is not so obvious, however.

In Ref. [7], we proposed a practical higher-order kinetic scheme for the compressible Navier–Stokes equation. The method for constructing the kinetic scheme developed there is directly related to the gasdynamic equation and the relation between the resulting scheme and the gasdynamic equation is transparent by construction. As by-products, the intrinsic error of the Pullin scheme for the Euler equation and that of the Chou–Baganoff scheme for

0021-9991/02 $35.00

the Navier–Stokes equation [2] are revealed; these methods are at most first-order accurate in time because of the lack of collision effect in the numerical flux.

The application range of the method in Ref. [7] is not restricted to the abovementioned gasdynamic equations. In the present paper, we first illustrate the principle of the method with the simple example of the linear advection equation, where no special knowledge of kinetic theory is necessary. It will be shown theoretically and numerically that the accuracy of the kinetic scheme is improved by the inclusion of collision effects in the numerical flux. Next we review the kinetic scheme developed in Ref. [7] and give some comments on the abovementioned plausible scenario. The Prendergast–Xu method [13] is known as the kinetic method that takes account of the collision effect explicitly in the numerical flux. Although it yields better results than the Chou–Bagnoff method in the viscous boundary layer problem [22], its relation to the gasdynamic equation and its order of accuracy are not clear from the derivation. We also refer to the legitimacy of the newest version of the scheme [22].

2. PRINCIPLE OF THE RAILROAD METHOD

2.1. Construction of the Railroad

The method of Ref. [7], which we will hereafter refer to as the *railroad* method, is applicable to the construction of kinetic schemes for various evolutionary equations (systems). For a clear understanding of the principle, we start with the simple example of the Cauchy problem of the linear advection equation,

$$\frac{\partial u(x,\,t)}{\partial t} + c\frac{\partial u(x,\,t)}{\partial x} = 0, \tag{1}$$

$$u(x,0) = u_0(x), \tag{2}$$

where c is a constant. First we introduce the distribution function $f(x,\,t,\,\zeta)$ and define the macroscopic variable $u(x,t)$ as a moment of f. For example, we choose

$$u(x,t) = \int_{-\infty}^{\infty} f(x,t,\zeta)\,d\zeta. \tag{3}$$

In a manner similar to the Chapman–Enskog expansion in kinetic theory, we consider the distribution function that depends on the space variable x and the time t only through their macroscopic variable u. For example, we choose

$$f(x,t,\zeta) = \frac{u(x,\,t)}{\sqrt{\pi}}\exp[-(\zeta - c)^2], \tag{4}$$

which is compatible with Eq. (3). Next we consider the distribution function (4) with a macroscopic variable that satisfies Eq. (1). We substitute the distribution function (4) into $(\partial_t + \zeta\,\partial_x)f$ and covert $\partial_t u$ in the result to $\partial_x u$ using Eq. (1). Then, we have

$$\frac{\partial f}{\partial t} + \zeta\frac{\partial f}{\partial x} = \frac{(\zeta - c)}{\sqrt{\pi}}\exp[-(\zeta - c)^2]\frac{\partial u}{\partial x}. \tag{5}$$

Equation (5) is merely the result of computation. From now on, we regard it together with the definition of u, Eq. (3), as the evolutionary equation for f. If $u(x,t)$ is the solution of

Cauchy problem (1) and (2), then the distribution function (4) is the solution of Cauchy problem of the kinetic equation (5) with Eq. (3) from the initial condition

$$f(x, 0, \zeta) = \frac{u_0(x)}{\sqrt{\pi}} \exp[-(\zeta - c)^2]. \tag{6}$$

The Cauchy problem of the kinetic equation (5) from the initial condition (6) is the railroad; the solution of the macroscopic equation (1) is obtained as the moment of the solution of the kinetic equation. The above procedure relies on the assumption of uniqueness of the solution of the Cauchy problem for f besides the natural assumption of the existence and uniqueness of the solution of the macroscopic equation.

2.2. Simplification of Kinetic Equation

In the railroad method, the solution of the macroscopic equation is obtained from that of the kinetic equation. The accuracy of u depends on that of f and the computation of the collision term is the key. If the collision term satisfies a certain condition, we can simplify its computation as shown in the following.

The solution of Cauchy problem for the kinetic equation (5) is formally expressed in integral form along its characteristic line as

$$f(x, \Delta t, \zeta) = f(x - \Delta t\zeta, 0, \zeta) + \int_0^{\Delta t} Q[f](x-(\Delta t - \tau)\zeta, \tau, \zeta)\, d\tau, \tag{7}$$

where

$$Q[f](x, t, \zeta) = \frac{(\zeta - c)}{\sqrt{\pi}} \exp[-(\zeta - c)^2]\frac{\partial u}{\partial x}. \tag{8}$$

Then $u(x,\ \Delta t)$ is given by

$$u(x,\ \Delta t) = \int_{-\infty}^{\infty} f(x - \Delta t\zeta, 0, \zeta)\, d\zeta + \int_{-\infty}^{\infty}\int_0^{\Delta t} Q[f](x-(\Delta t - \tau)\zeta, \tau, \zeta)\, d\tau\, d\zeta. \tag{9}$$

By applying the trapezoid rule to the integral with respect to τ, we have

$$\begin{aligned} u(x, \Delta t) = {} & \int_{-\infty}^{\infty} f(x - \Delta t\zeta, 0, \zeta)\, d\zeta + \frac{\Delta t}{2}\int_{-\infty}^{\infty} [Q[f](x, \Delta t, \zeta) \\ & + Q[f](x, 0, \zeta)]\, d\zeta - \frac{\Delta t^2}{2}\int_{-\infty}^{\infty} \zeta \frac{\partial Q[f](x, 0, \zeta)}{\partial x}\, d\zeta + O(\Delta t^3). \end{aligned} \tag{10}$$

The contribution of $Q[f]$ to $u(x,\ \Delta t)$ is $O(\Delta t)$ and this term is indispensable generally. If the definition of u and the functional form of $f(u(x, t), \zeta)$ are chosen so that the resulting $Q[f]$ satisfies the orthogonality condition

$$\int_{-\infty}^{\infty} Q[f](x, t, \zeta)\, d\zeta = 0, \tag{11}$$

which is satisfied in the present example, then the contribution of $Q[f]$ to $u(x, \Delta t)$ becomes $O(\Delta t^2)$. In this case, we can simplify it. In fact, if we employ the collisionless equation

$$\frac{\partial f}{\partial t} + \zeta\frac{\partial f}{\partial x} = 0, \tag{12}$$

the error becomes $O(\Delta t^2)$. That is, the intrinsic error of the kinetic scheme which is based on the Cauchy problem of the collisionless equation is $O(\Delta t^2)$ and the accuracy is at most first order in time. As shown in Section 2.3, the initial condition in the form of Eq. (6) is reconstructed using the cell-averaged values of u at the beginning of every time step. Thus, u is not obtained as the moment of the solution of the collisionless equation (12) even if the collisionless equation is employed in the computation of the evolution step.

2.3. Numerical Art

In this section, we employ the railroad method to derive the finite volume scheme for Eq. (1). For simplicity we consider the case where the space region is divided into cells of uniform size. Integrating Eq. (5) over $(-\infty, \infty)$ for ζ, over each cell $(s_{i-1/2}, s_{i+1/2})$ for x, and over the time interval $(0, \Delta t)$, and making use of the orthogonality of $Q[f]$, we have

$$U_i(\Delta t) = U_i(0) - \frac{1}{\Delta x}\big(F_{i+1/2} - F_{i-1/2}\big), \tag{13}$$

where

$$U_i(t) = \frac{1}{\Delta x}\int_{s_{i-1/2}}^{s_{i+1/2}}\int_{-\infty}^{\infty} f(x, t, \zeta)\, d\zeta\, dx, \tag{14}$$

$$\begin{aligned} F_{i+1/2} &= \int_0^{\Delta t}\int_{-\infty}^{\infty} \zeta f\big(s_{i+1/2}, t, \zeta\big)\, d\zeta\, dt, \\ \Delta x &= s_{i+1/2} - s_{i-1/2}. \end{aligned} \tag{15}$$

The cell-averaged value U_i represents the value of u at $x = s_i \equiv (s_{i+1/2} + s_{i-1/2})/2$. The numerical flux $F_{i+1/2}$ is computed from an approximate solution of the initial value problem (5) and (6). If we employ

$$f\big(s_{i+1/2}, t, \zeta\big) = f\big(s_{i+1/2} - t\zeta, 0, \zeta\big), \tag{16}$$

which is the solution of the collisionless equation (12), the error of $F_{i+1/2}$ becomes $O(\Delta t^2)$ because $Q[f]$ is multiplied by ζ in the integral and the contribution does not vanish. Thus, we have the first-order-accurate flux. In the actual construction of the scheme, the first term or the first two terms in the Taylor expansion of $f(s_{i+1/2} - t\zeta, 0, \zeta)$ suffice:

$$f\big(s_{i+1/2}, t, \zeta\big) = f\big(s_{i+1/2}, 0, \zeta\big), \tag{17}$$

$$f\big(s_{i+1/2}, t, \zeta\big) = f\big(s_{i+1/2}, 0, \zeta\big) - t\zeta\,\frac{\partial f\big(s_{i+1/2}, 0, \zeta\big)}{\partial x}. \tag{18}$$

If the contribution of $Q[f]$ is retained up to the order of t, i.e.,

$$f\big(s_{i+1/2}, t, \zeta\big) = f\big(s_{i+1/2}, 0, \zeta\big) - t\zeta\frac{\partial f}{\partial x}\big(s_{i+1/2}, 0, \zeta\big) + tQ[f]\big(s_{i+1/2}, 0, \zeta\big), \tag{19}$$

we have the second-order-accurate flux.

The scheme becomes apparent when the reconstruction of the initial data is specified. In the case of the reconstruction that allows the discontinuity at the cell boundaries, the

numerical flux splits into two parts according to the direction of the characteristic line (the sign of ζ),

$$F_{i+1/2} = F^{+}_{i+1/2} + F^{-}_{i+1/2}, \tag{20}$$

where

$$F^{\pm}_{i+1/2} = \int_0^{\Delta t} \int_{\zeta \gtrless 0} \zeta f\left(s_{i+1/2} \mp 0, t, \zeta\right) d\zeta \, dt. \tag{21}$$

The numerical flux $F^{\pm}_{i+1/2}$ for Eq. (19) consists of three parts,

$$F^{\pm}_{i+1/2} = \Delta t G^{\pm}_{i+1/2} - \frac{\Delta t^2}{2}\left(H^{\pm}_{i+1/2} - K^{\pm}_{i+1/2}\right), \tag{22}$$

$$\begin{aligned} G^{\pm}_{i+1/2} &= \int_{\zeta \gtrless 0} \zeta f\left(s_{i+1/2} \mp 0, 0, \zeta\right) d\zeta \\ &= \frac{1}{2} u\left(s_{i+1/2} \mp 0, 0\right)\left[\pm \frac{e^{-c^2}}{\sqrt{\pi}} + c(1 \pm \mathrm{Erf}(c))\right], \end{aligned} \tag{23}$$

$$\begin{aligned} H^{\pm}_{i+1/2} &= \int_{\zeta \gtrless 0} \zeta^2 \frac{\partial f}{\partial x}\left(s_{i+1/2} \mp 0, 0, \zeta\right) d\zeta \\ &= \frac{1}{2}\frac{\partial u}{\partial x}\left(s_{i+1/2} \mp 0, 0\right)\left[\pm \frac{c e^{-c^2}}{\sqrt{\pi}} + \left(c^2 + \frac{1}{2}\right)(1 \pm \mathrm{Erf}(c))\right], \end{aligned} \tag{24}$$

$$\begin{aligned} K^{\pm}_{i+1/2} &= \int_{\zeta \gtrless 0} \zeta Q[f]\left(s_{i+1/2} \mp 0, 0, \zeta\right) d\zeta \\ &= \frac{1}{4}\frac{\partial u}{\partial x}\left(s_{i+1/2} \mp 0, 0\right)(1 \pm \mathrm{Erf}(c)), \end{aligned} \tag{25}$$

where

$$\mathrm{Erf}(c) = \frac{2}{\sqrt{\pi}} \int_0^c e^{-s^2} \, ds.$$

The numerical flux $F^{\pm}_{i+1/2}$ for Eq. (17) is given by $\Delta t G^{\pm}_{i+1/2}$ and that for Eq. (18) is given by $\Delta t G^{\pm}_{i+1/2} - (\Delta t^2/2) H^{\pm}_{i+1/2}$.

The role of the collision effect can be demonstrated without numerical computation in the case of continuous piecewise linear distribution:

Reconstruction-I

$$u(x, 0) = \begin{cases} U_i(0) + \frac{U_{i+1}(0) - U_i(0)}{\Delta x}(x - s_i), & \text{for } s_i \le x \le s_{i+1/2}, \\ U_i(0) + \frac{U_i(0) - U_{i-1}(0)}{\Delta x}(x - s_i), & \text{for } s_{i-1/2} \le x \le s_i. \end{cases} \tag{26}$$

In this case, we need not divide the numerical flux since $u(s_{i+1/2} + 0, 0) = u(s_{i+1/2} - 0, 0) = (U_i(0) + U_{i+1}(0))/2$ and $(\partial u/\partial x)(s_{i+1/2} + 0, 0) = (\partial u/\partial x)(s_{i+1/2} - 0, 0) = (U_{i+1} - U_i(0))/\Delta x$. The numerical fluxes for Eqs. (17), (18), and (19) are readily obtained from Eqs. (23), (24), and (25):

$$F_{i+1/2} = c\Delta t u\left(s_{i+1/2}, 0\right), \tag{27}$$

$$F_{i+1/2} = c\Delta t u\big(s_{i+1/2}, 0\big) - \left(c^2 + \frac{1}{2}\right)\frac{\Delta t^2}{2}\frac{\partial u\big(s_{i+1/2}, 0\big)}{\partial x}, \tag{28}$$

$$F_{i+1/2} = cu\big(s_{i+1/2}, 0\big)\Delta t - c^2\frac{\Delta t^2}{2}\frac{\partial u\big(s_{i+1/2}, 0\big)}{\partial x}. \tag{29}$$

The numerical schemes corresponding to Eq. (27), (28), and (29) are, respectively,

$$U_i(\Delta t) = U_i(0) - \frac{c\Delta t}{2\Delta x}[U_{i+1}(0) - U_{i-1}(0)], \tag{30}$$

$$U_i(\Delta t) = U_i(0) - \frac{c\Delta t}{2\Delta x}[U_{i+1}(0) - U_{i-1}(0)] + \left(c^2 + \frac{1}{2}\right)\frac{\Delta t^2}{2\Delta x^2}[U_{i+1}(0) - 2U_i(0) + U_{i-1}(0)], \tag{31}$$

and

$$U_i(\Delta t) = U_i(0) - \frac{c\Delta t}{2\Delta x}[U_{i+1}(0) - U_{i-1}(0)] + \frac{c^2\Delta t^2}{2\Delta x^2}[U_{i+1}(0) - 2U_i(0) + U_{i-1}(0)]. \tag{32}$$

Scheme (30) is called the FTCS (forward time and central space) scheme and is unconditionally unstable. The second scheme (31) is first-order accurate in time and is stable under the condition $(c^2 + 1/2)^{1/2}\Delta t < \Delta x$. The derivative of f contributes to the compensation for the negative artificial viscosity of the FTCS scheme. In scheme (32) the collision term $Q[f]$ acts to remove an excess of dissipation. That is, by taking account of the collision effect correctly, the railroad reaches the well-known Lax–Wendroff scheme (32), which is second-order accurate in space and time and is stable under the condition $c\Delta t < \Delta x$. We remark that the lack of stability is not peculiar to the choice of Eq. (17). For example, let us consider the case of the piecewise constant initial distribution; i.e., the vlaue of u inside the ith cell is equal to the cell-averaged value U_i. Then, the numerical flux is given by $F_{i+1/2} = \Delta t(G^+_{i+1/2} + G^-_{i+1/2})$ and the resulting scheme is

$$U_i(\Delta t) = U_i(0) - \frac{c\Delta t}{2\Delta x}[U_{i+1}(0) - U_{i-1}(0)] + \frac{A(c)\Delta t}{2\Delta x}[U_{i+1}(0) - 2U_i(0) + U_{i-1}(0)], \tag{33}$$

where

$$A(c) = \frac{e^{-c^2}}{\sqrt{\pi}} + c\mathrm{Erf}(c). \tag{34}$$

This scheme is stable under the condition $\max[A(c), c^2/A(c)]\Delta t < \Delta x$.

Finally, we proceed to the numerical example. To demonstrate the influence of the reconstruction step as well as that of the evolution step, we prepare two solutions for the evolution step, Eqs. (18) and (19), and three piecewise linear reconstructions, Reconstruction-I defined in Eq. (26) and Reconstruction-II and Reconstruction-III defined as

Reconstruction-II

$$u(x, 0) = U_i(0) + \frac{U_{i+1}(0) - U_{i-1}(0)}{2\Delta x}(x - s_i), \qquad \big(s_{i-1/2} \le x \le s_{i+1/2}\big), \tag{35}$$

Reconstruction-III

$$
\begin{aligned}
u(x,0) &= U_i(0) + S_i(0)(x - s_i), \qquad \left(s_{i-1/2} \le x \le s_{i+1/2}\right),\\
S_i &= \frac{1}{\Delta x}\mathrm{minmod}(V_i, W_i),\\
V_i &= U_{i+1} - U_i - \frac{1}{2}\mathrm{minmod}(U_{i+1} - 2U_i + U_{i-1}, U_{i+2} - 2U_{i+1} + U_i),\\
W_i &= U_i - U_{i-1} + \frac{1}{2}\mathrm{minmod}(U_{i+1} - 2U_i + U_{i-1}, U_i - 2U_{i-1} + U_{i-2}),
\end{aligned}
\tag{36}
$$

where the minmod function is defined by

$$
\mathrm{minmod}(x,y) = \begin{cases} m(x,y), & \text{for } xy > 0,\\ 0, & \text{for } xy \le 0, \end{cases}
\qquad
m(x,y) = \begin{cases} y, & \text{for } |y| \le |x|,\\ x, & \text{for } |y| > |x|. \end{cases}
$$

Equation (35) is the Van Leer reconstruction with the central difference approximation of the slope [21] and Eq. (36) is that with the Harten–Osher slope [5]. The demonstration problems are taken from Laney's textbook [6] (Test Cases 1–3), where the Cauchy problem of the linear advection equation (1) with $c = 1$ is solved for $-1 \le x \le 1$ under the periodic condition $u(1 + s, t) = u(-1 + s, t)$. The initial condition and the computational parameters are as follows:

Test Case 1

$$
u(x,0) = -\sin(\pi x), \qquad \Delta x = 0.05, \qquad \frac{\Delta t}{\Delta x} = 0.8;
$$

Test Case 2

$$
u(x,0) = \begin{cases} 1 & \text{for } |x| < \frac{1}{3},\\ 0 & \text{for } \frac{1}{3} \le |x| \le 1, \end{cases}
\qquad \Delta x = 0.05, \qquad \frac{\Delta t}{\Delta x} = 0.8;
$$

Test Case 3

$$
u(x,0) = \begin{cases} 1 & \text{for } |x| < \frac{1}{3},\\ 0 & \text{for } \frac{1}{3} \le |x| \le 1, \end{cases}
\qquad \Delta x = \frac{1}{300}, \qquad \frac{\Delta t}{\Delta x} = 0.8.
$$

The results for the sets Eq. (18), Reconstruction-II; Eq. (19), Reconstruction-I (the Lax–Wendroff); and Eq. (19), Reconstruction-II in Test Cases 1–3 are shown in Figs. 1–3. The schemes for Eq. (19) capture the sinusoid's shape and the amplitude well (Fig. 1). While the Lax–Wendroff scheme (Reconstructon-I) has a visible lagging phase error, it is nearly invisible for Reconstruction-II. The scheme without the collision effect captures the sinusoid's shape with invisble phase error but the amplitude is very poor; the lack of the collision effect causes the large artificial viscosity. As seen in Fig. 2, the result of the scheme without the collision effect is smeared although it is free of overshoots or undershoots. The schemes with the collision effect have spurious oscillations but Reconstruction-II gives a better result than Reconstruction-I. The same tendency is observed in Test Case 3 (Fig. 3). The results for the sets Eq. (18), Reconstruction-III and Eq. (19), Reconstruction-III in Test Cases 1–3 are shown in Figs. 4–6. Owing to the well-established reconstruction technique,

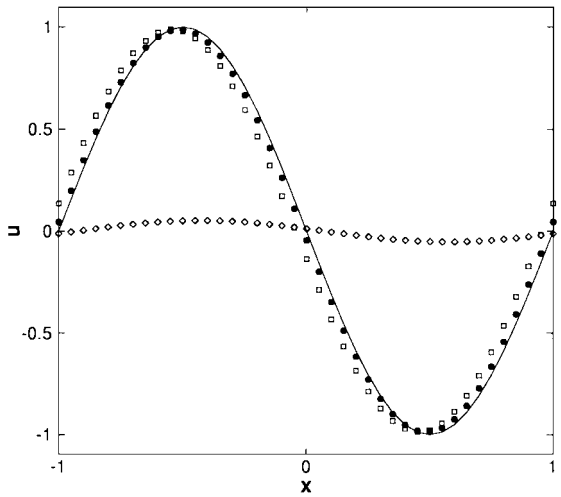

FIG. 1. Comparison of $u(x, 30)$ in Test Case 1. The solid line indicates the exact solution and the symbols $\diamond$, $\square$, and $\bullet$ indicate the results of Eq. (18), Reconstruction-II; Eq. (19), Reconstruction-I (Lax–Wendroff); and Eq. (19), Reconstruction-II, respectively.

the result of the scheme based on Eq. (19) is improved dramatically in Test Cases 2 and 3 (Figs. 5 and 6) and the side effect of this strong medicine for the purpose of suppressing the spurious oscillations is not visible in Test Case 1 (Fig. 4). If the slope defined by Eq. (36) is replaced by that of the Van Leer limiter

$$S_i = \begin{cases} \frac{2(U_{i+1}-U_i)(U_i-U_{i-1})}{\Delta x(U_{i+1}-U_{i-1})}, & \text{for } (U_{i+1}-U_i)(U_i-U_{i-1}) > 0, \\ 0, & \text{for } (U_{i+1}-U_i)(U_i-U_{i-1}) \le 0, \end{cases} \tag{37}$$

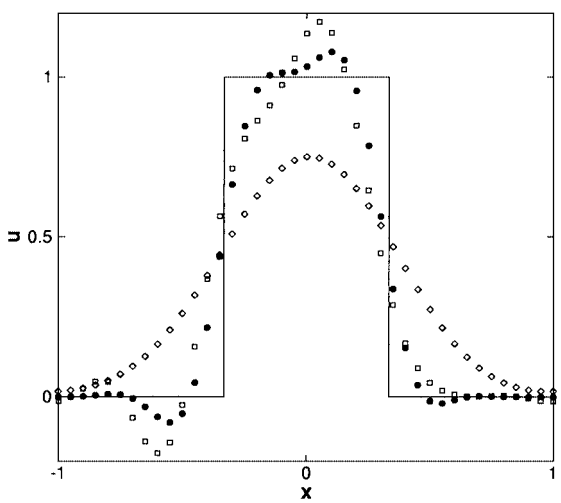

FIG. 2. Comparison of $u(x, 4)$ in Test Case 2. The solid line indicates the exact solution and the symbols $\diamond$, $\square$, and $\bullet$ indicate the results of Eq. (18), Reconstruction-II; Eq. (19), Reconstruction-I (Lax–Wendroff); and Eq. (19), Reconstruction-II, respectively.

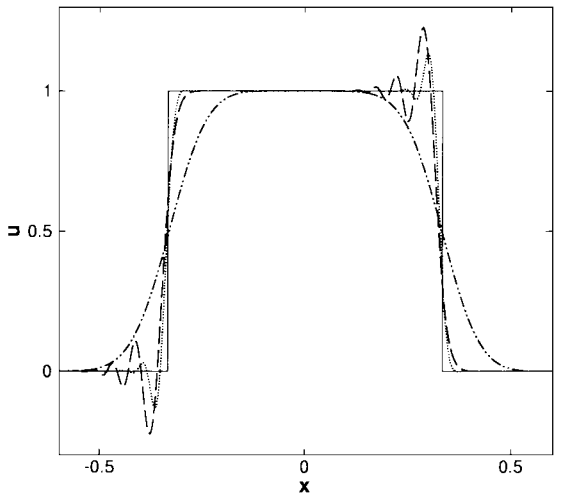

FIG. 3. Comparison of $u(x, 4)$ in Test Case 3. The solid line indicates the exact solution, – ·· – indicates the result of Eq. (18), Reconstruction-II, — — indicates the result of Eq. (19), Reconstruction-I (Lax–Wendroff), and · · · · · indicates the result of Eq. (19), Reconstruction-II.

the side effect, the clipping, becomes visible in Test Case 1 (no figure). The result of the scheme without the collision effect is nearly independent of the reconstruction in all cases. The intrinsic error of the scheme spoils the effectiveness of the good medicine.

The properties of the scheme, such as the accuracy, stability, and so on, depend not only on the evolution step, with which the railroad method is concerned, but also on the reconstruction step. From the above consideration and demonstration, we find that the improvement in the evolution step under the rich reconstruction step makes the scheme stable or more accurate but the improvement in the reconstruction step under the poor evolution step is meaningless or makes the scheme unstable.

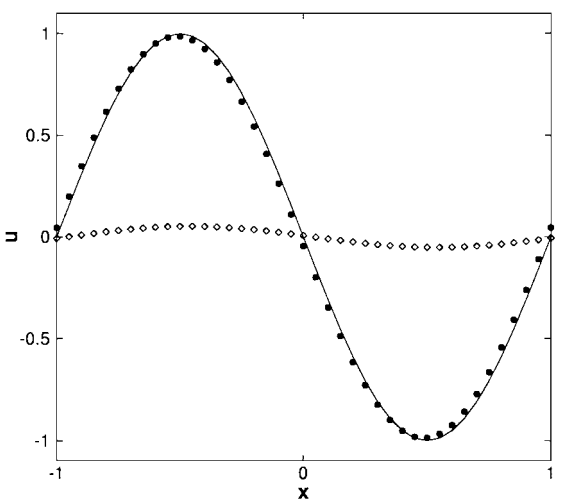

FIG. 4. Comparison of $u(x, 30)$ in Test Case 1. The solid line indicates the exact solution and the symbols ◇ and ● indicate the results of Eq. (18), Reconstruction-III and Eq. (19), Reconstruction-III, respectively.

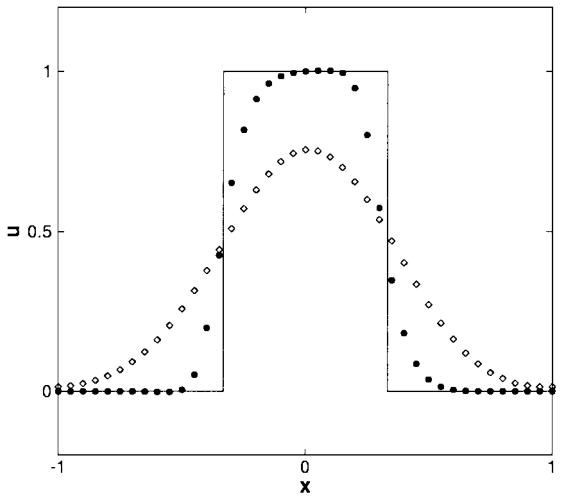

FIG. 5. Comparison of $u(x, 4)$ in Test Case 2. The solid line indicates the exact solution and the symbols $\diamond$ and $\bullet$ indicate the results of Eq. (18), Reconstruction-III and Eq. (19), Reconstruction-III, respectively.

3. APPLICATION TO GASDYNAMIC EQUATIONS

In this section we apply the railroad method to the compressible Euler equation and the compressible Navier–Stokes equation derived from the Boltzmann equation by the Chapman–Enskog expansion. The reason why we consider the Chapman–Enskog expansion is that the railroad is buried in the expansion results and the resulting scheme can be employed together with the slip boundary condition as the solver of the Boltzmann equation for small Knudsen numbers, although the Navier–Stokes equation does not always give the correct description of gas behavior even in the continuum limit [15] and the legitimacy of this Boltzmann solver should be checked by the systematic asymptotic analysis of the

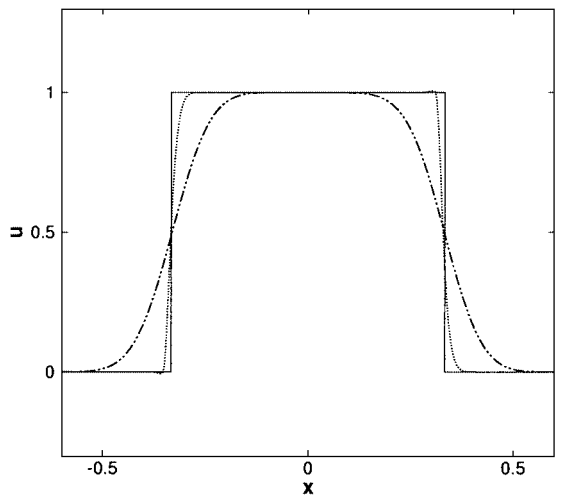

FIG. 6. Comparison of $u(x, 4)$ in Test Case 3. The solid line indicates the exact solution – ·· – indicates the result of Eq. (18), Reconstruction-III, and · · · · · indicates the result of Eq. (19), Reconstruction-III.

Boltzmann equation. For the asymptotic analyses of the Boltzmann equation, see Refs. [15, 16] and the references therein. For the slip boundary condition obtained by modern analyses of kinetic theory, the reader is referred to Refs. [17, 18] (BGK) and Refs. [8, 19] (hard-sphere molecules).

3.1. Chapman–Enskog Expansion

Before proceeding to the application of the railroad method to the gasdynamic equation systems, we explain the Chapman–Enskog expansion for the Boltzmann equation according to the excellent review by Grad [4].

The main notation is summarized as follows: L is the reference length of the system under consideration; ρ_0 and T_0 are the reference density and temperature; l_0 is the mean free path of the gas molecules for the equilibrium state at rest with density ρ_0 and temperature T_0; $\epsilon = \sqrt{\pi} l_0/(2L)$; Lx_i is the space coordinate system; $(2RT_0)^{1/2}\zeta_i$ is the molecular velocity, where R is the specific gas constant; $L(2RT_0)^{-1/2}\,t$ is the time; $\rho_0(2RT_0)^{-3/2} f(x_i, t, \zeta_i)$ is the distribution function of gas molecules; $\rho_0\rho$, $(2RT_0)^{1/2}u_i$, and $T_0 T$ are the density, flow velocity, and temperature of the gas, respectively.

The nondimensional Boltzmann equation is written in the form

$$\frac{\partial f(x_i, t, \zeta_i)}{\partial t} + \zeta_j \frac{\partial f(x_i, t, \zeta_i)}{\partial x_j} = \frac{1}{\epsilon} J(f, f)(x_i, t, \zeta_i), \tag{38}$$

where J is the collision operator and its definition is given elsewhere, e.g., Refs. [1] and [20]. In the Chapman–Enskog expansion, the situation where $0 < \epsilon \ll 1$ and $\partial_t f \sim \partial_x f \sim f$ is considered and the distribution function f is assumed to be in the form

$$f = f(\boldsymbol{h}, D\boldsymbol{h}, \zeta_i, \epsilon), \tag{39}$$

where the components of the vector $\boldsymbol{h}$ represent ρ, u_i, and T, i.e., $\boldsymbol{h} =^t (\rho, u_i, T)$, and D means the differential operators with respect to x_i. The macroscopic variables $\tilde{\boldsymbol{h}} =^t (\rho, \rho u_i, 3\rho T/2 + \rho u_k^2)$ are given by the moment of f,

$$\tilde{\boldsymbol{h}} = \int_{-\infty}^{\infty}\int_{-\infty}^{\infty}\int_{-\infty}^{\infty} \psi f \, d\zeta_1 \, d\zeta_2 \, d\zeta_3, \tag{40}$$

where $\psi =^t (\psi_0, \psi_1, \psi_2, \psi_3, \psi_4) =^t (1, \zeta_1, \zeta_2, \zeta_3, \zeta_k^2)$. The distribution function f is assumed to depend on x_i and t only through $\boldsymbol{h}$ and $D\boldsymbol{h}$. It is also assumed that the time derivatives of the macroscopic variables are in the form

$$\frac{\partial \boldsymbol{h}}{\partial t} = \boldsymbol{\Phi}(\boldsymbol{h}, D\boldsymbol{h}, \epsilon). \tag{41}$$

The distribution function f and the time derivatives of the macroscopic variables $\boldsymbol{\Phi}$ are expanded into the power series of ϵ:

$$f(\boldsymbol{h}, D\boldsymbol{h}, \epsilon) = f_0(\boldsymbol{h}, D\boldsymbol{h}) + \epsilon f_1(\boldsymbol{h}, D\boldsymbol{h}) + \epsilon^2 f_2(\boldsymbol{h}, D\boldsymbol{h}) + \cdots, \tag{42}$$

$$\boldsymbol{\Phi}(\boldsymbol{h}, D\boldsymbol{h}, \epsilon) = \boldsymbol{\Phi}_0(\boldsymbol{h}, D\boldsymbol{h}) + \epsilon \boldsymbol{\Phi}_1(\boldsymbol{h}, D\boldsymbol{h}) + \epsilon^2 \boldsymbol{\Phi}_2(\boldsymbol{h}, D\boldsymbol{h}) + \cdots, \tag{43}$$

Substituting Eqs. (42) and (43) into the Boltzmann equation and arranging the result in the order of power of ϵ (the operator J is bilinear), we have

$$0 = J(f_0, f_0), \tag{44}$$

$$\sum_{l+m=k-1} \left(\frac{\partial f_l}{\partial \boldsymbol{h}} \boldsymbol{\Phi}_m + \frac{\partial f_l}{\partial D\boldsymbol{h}} D\boldsymbol{\Phi}_m \right) + \zeta_j \frac{\partial f_{k-1}}{\partial x_j} = \sum_{l+m=k} J(f_l, f_m) \quad (k \geq 1). \tag{45}$$

The sequence of integral equations are solved from the lowest order under the constraint

$$\int_{-\infty}^{\infty}\int_{-\infty}^{\infty}\int_{-\infty}^{\infty} \psi f_0 \, d\zeta_1 \, d\zeta_2 \, d\zeta_3 = \tilde{\boldsymbol{h}}, \tag{46}$$

$$\int_{-\infty}^{\infty}\int_{-\infty}^{\infty}\int_{-\infty}^{\infty} \psi f_k \, d\zeta_1 \, d\zeta_2 \, d\zeta_3 = 0 \quad (k \geq 1). \tag{47}$$

Since J satisfies the orthogonality condition

$$\int_{-\infty}^{\infty}\int_{-\infty}^{\infty}\int_{-\infty}^{\infty} \psi J(f, g) \, d\zeta_1 \, d\zeta_2 \, d\zeta_3 = 0, \tag{48}$$

for any f and g, the left-hand side of Eq. (45) must be orthogonal to ψ, from which $\boldsymbol{\Phi}_k (k = 0, 1, 2, \ldots)$ are determined.

The solution of Eq. (44) is the local Maxwellian

$$f_0 = \frac{\rho}{(\pi T)^{3/2}} \exp(-C^2), \tag{49}$$

where $C^2 = C_k^2$ and $C_i = (\zeta_i - u_i)/T^{1/2}$. Since f_0 does not include any derivative of a macroscopic variable, Eq. (45) for $k = 1$ becomes

$$\frac{\partial f_0}{\partial \boldsymbol{h}} \boldsymbol{\Phi}_0 + \zeta_j \frac{\partial f_0}{\partial x_j} = 2J(f_0, f_1). \tag{50}$$

From the compatibility condition of Eq. (50), we obtain the explicit form of $\boldsymbol{\Phi}_0$. Then,

$$\frac{\partial \boldsymbol{h}}{\partial t} = \boldsymbol{\Phi}_0 \tag{51}$$

constitutes the compressible Euler system. The explicit form of Eq. (50) is

$$\left[2\left(C_i C_j - \frac{C^2}{3}\delta_{ij} \right) \frac{\partial u_i}{\partial x_j} + \frac{C_i}{T^{1/2}} \left(C^2 - \frac{5}{2} \right) \frac{\partial T}{\partial x_i} \right] f_0 = 2J(f_0, f_1). \tag{52}$$

The distribution function f_1, which gives the viscosity and thermal conductivity, is obtained as the solution of the the integral equation (52) under the condition (47). For hard-sphere molecules, f_1 is given by

$$f_1 = -\frac{1}{\rho T^{1/2}} \left[\left(C_i C_j - \frac{C^2}{3}\delta_{ij} \right) B(C) \frac{\partial u_i}{\partial x_j} + \frac{C_i}{T^{1/2}} A(C) \frac{\partial T}{\partial x_i} \right] f_0, \tag{53}$$

where the functions $A(C)$ and $B(C)$ are the solutions of the integral equations related to the linearized collision operator and their accurate data are obtained in Refs. [9–11]. [The

functions $\nu(\zeta)$ in Eqs. (A1)–(A5) in Ref. [9] should be $2\sqrt{2}\nu(\zeta)$.] The derivatives in f_1 are first order, i.e., $f_1 = f_1(\boldsymbol{h}, \nabla\boldsymbol{h}, \zeta_i)$, and Eq. (45) for $k = 2$ becomes

$$\frac{\partial f_0}{\partial \boldsymbol{h}}\boldsymbol{\Phi}_1 + \frac{\partial f_1}{\partial \boldsymbol{h}}\boldsymbol{\Phi}_0 + \frac{\partial f_1}{\partial \nabla \boldsymbol{h}}\nabla\boldsymbol{\Phi}_0 + \zeta_j \frac{\partial f_1}{\partial x_j} = 2J(f_0, f_2) + J(f_1, f_1). \tag{54}$$

The compatibility condition of Eq. (54) determines $\boldsymbol{\Phi}_1$. Then,

$$\frac{\partial \boldsymbol{h}}{\partial t} = \boldsymbol{\Phi}_0 + \epsilon\boldsymbol{\Phi}_1 \tag{55}$$

constitutes the compressible Navier–Stokes equation sytem.

We summarize the results of the Chapman–Enskog expansion for the BGK model equation

$$\frac{\partial f}{\partial t} + \zeta_j \frac{\partial f}{\partial x_j} = \frac{1}{\epsilon}\rho(f_0 - f), \tag{56}$$

where f_0 is the local Maxwellian defined by Eqs. (49) and (40). The equation corresponding to Eq. (50) is

$$\frac{\partial f_0}{\partial \boldsymbol{h}}\boldsymbol{\Phi}_0 + \zeta_j \frac{\partial f_0}{\partial x_j} = -\rho f_1. \tag{57}$$

From the condition (47) for $k = 1$, we have $\boldsymbol{\Phi}_0$, which is the same as that for the Boltzmann equation. Then, Eq. (57) becomes

$$\left[2\left(C_i C_j - \frac{C^2}{3}\delta_{ij}\right)\frac{\partial u_i}{\partial x_j} + \frac{C_i}{T^{1/2}}\left(C^2 - \frac{5}{2}\right)\frac{\partial T}{\partial x_i}\right] f_0 = -\rho f_1, \tag{58}$$

from which we readily obtain f_1. The equation corresponding to Eq. (54) is

$$\frac{\partial f_0}{\partial \boldsymbol{h}}\boldsymbol{\Phi}_1 + \frac{\partial f_1}{\partial \boldsymbol{h}}\boldsymbol{\Phi}_0 + \frac{\partial f_1}{\partial \nabla \boldsymbol{h}}\nabla\boldsymbol{\Phi}_0 + \zeta_j \frac{\partial f_1}{\partial x_j} = -\rho f_2, \tag{59}$$

and we have $\boldsymbol{\Phi}_1$ from the condition (47) for $k = 2$. Then we have the compressible Navier–Stokes system (55), which is different from that the Boltzmann equation only in the viscosity and the thermal conductivity.

Finally, in summary, the compressible Navier–Stokes equation derived from the Boltzmann equation for hard-sphere molecules and that from the BGK equation are

$$\frac{\partial}{\partial t}\begin{pmatrix} \rho \\ \rho u_i \\ \rho\left[\frac{3}{2}T + u_k^2\right] \end{pmatrix} + \frac{\partial}{\partial x_j}\begin{pmatrix} \rho u_j \\ \rho u_i u_j + \frac{1}{2}P_{ij} \\ \rho\left[\frac{3}{2}T + u_k^2\right]u_j + P_{kj}u_k + Q_j \end{pmatrix} = 0, \tag{60}$$

where

$$P_{ij} = P\delta_{ij} - \gamma_1 \epsilon T^a \left(\frac{\partial u_i}{\partial x_j} + \frac{\partial u_j}{\partial x_i} - \frac{2}{3}\frac{\partial u_k}{\partial x_k}\delta_{ij}\right), \tag{61}$$

$$Q_i = -\frac{5}{4}\gamma_2 \epsilon T^a \frac{\partial T}{\partial x_i}, \tag{62}$$

and γ_i and a are constants: $\gamma_1 = 1.270042427$, $\gamma_2 = 1.922284066$, and $a = 1/2$ for hard-sphere molecules [9, 10, 20] and $\gamma_1 = \gamma_2 = a = 1$ for the BGK model [17, 18, 20].

3.2. Application to the Euler System

Applying the railroad method to the compressible Euler equation (51) can readily be done since all the necessary materials have already been prepared in the previous section. First we assume that the functional form of the distribution function is $f = f_0(\boldsymbol{h}(x_i, t), \zeta_i)$ and the macroscopic variable $\boldsymbol{h}$ satisfy the compressible Euler equation (51). Then, we have the kinetic equation

$$\frac{\partial f}{\partial t} + \zeta_j \frac{\partial f}{\partial x_j} = \frac{\partial f_0}{\partial \boldsymbol{h}} \boldsymbol{\Phi}_0 + \zeta_j \frac{\partial f_0}{\partial x_j} = 2J(f_0, f_1), \tag{63}$$

where the explicit expression of the right-hand side is given in Eq. (52). From the solution of Eq. (63) and the initial condition

$$f(x_i, 0, \zeta_i) = f_0(\boldsymbol{h}(x_i, 0), \zeta_i), \tag{64}$$

we have the solution of the compressible Euler equation.

Similarly to the linear advection equation studied in Section 2, the solution of the above kinetic equation can be expressed in integral form along its characteristic line. Owing to the orthogonality condition (48), $\tilde{\boldsymbol{h}}(x_i, \Delta t)$ is evaluated as

$$\begin{aligned}\tilde{\boldsymbol{h}}(x_i, \Delta t) = &\int_{-\infty}^{\infty}\int_{-\infty}^{\infty}\int_{-\infty}^{\infty} \psi f(x - \zeta_j \Delta t, 0, \zeta_i)\, d\zeta_1\, d\zeta_2\, d\zeta_3 - \Delta t^2 \frac{\partial}{\partial x_j} \\ &\times \int_{-\infty}^{\infty}\int_{-\infty}^{\infty}\int_{-\infty}^{\infty} \psi \zeta_j J(f_0, f_1)(x_i, 0, \zeta_i)\, d\zeta_1\, d\zeta_2\, d\zeta_3 + O(\Delta t^3). \end{aligned} \tag{65}$$

Equation (65) indicates that the error becomes $O(\Delta t^2)$ if we omit the term $J(f_0, f_1)$; the intrinsic error of the Pullin scheme for the compressible Euler equation, which is based on the Cauchy problem of the collisionless equation

$$\frac{\partial f}{\partial t} + \zeta_j \frac{\partial f}{\partial x_j} = 0, \tag{66}$$

from the initial condition (64), is $O(\Delta t^2)$, and thus, it is at most first-order accurate in time. Deshpande [3] and Perthame [12] have developed second-order kinetic schemes for the compressible Euler equation. Although the collisionless equation is employed, second-order accuracy is established by the brilliant modification of the initial data. As shown above, the intrinsic error of the scheme based on Eq. (63) is zero. That is, we can construct the second-order-accurate scheme by modifying the kinetic equation instead of the initial data.

If $2J(f_0, f_1)$ in Eq. (63) is replaced by the collision term of the Boltzmann equation $(1/\epsilon)J(f, f)$, the macroscopic variables are evaluated as

$$\tilde{\boldsymbol{h}}(x_i, \Delta t) = \int_{-\infty}^{\infty}\int_{-\infty}^{\infty}\int_{-\infty}^{\infty} \psi f(x - \zeta_j \Delta t, 0, \zeta_i)\, d\zeta_1\, d\zeta_2\, d\zeta_3 + O(\Delta t^3), \tag{67}$$

because of Eq. (44). Then, comparing Eq. (65) and Eq. (67), we find that the accuracy decreases except for the special case of $2J(f_0, f_1) = 0$, i.e., no gradient for u_i and T.

3.3. Application to the Compressible Navier–Stokes System

The application of the railroad method to the compressible Navier–Stokes equation (55) is as follows. First we consider the distribution function in the form

$$f = f_0(\boldsymbol{h}, \zeta_i) + \epsilon f_1(\boldsymbol{h}, \nabla \boldsymbol{h}, \zeta_i) \tag{68}$$

and assume that its macroscopic variables $\boldsymbol{h}$ satisfy Eq. (55). Then, we have

$$\frac{\partial f}{\partial t} + \zeta_j \frac{\partial f}{\partial x_j} = \frac{\partial f_0}{\partial \boldsymbol{h}} \boldsymbol{\Phi}_0 + \zeta_j \frac{\partial f_0}{\partial x_j} + \epsilon \left[\frac{\partial f_0}{\partial \boldsymbol{h}} \boldsymbol{\Phi}_1 + \frac{\partial f_1}{\partial \boldsymbol{h}} \boldsymbol{\Phi}_0 + \frac{\partial f_1}{\partial \nabla \boldsymbol{h}} \nabla \boldsymbol{\Phi}_0 + \zeta_j \frac{\partial f_1}{\partial x_j} \right] + \epsilon^2 \left[\frac{\partial f_1}{\partial \boldsymbol{h}} \boldsymbol{\Phi}_1 + \frac{\partial f_1}{\partial \nabla \boldsymbol{h}} \nabla \boldsymbol{\Phi}_1 \right]. \tag{69}$$

All the terms in the right-hand side of Eq. (69) are buried in the results of the Chapman–Enskog expansion. Equation (69) is rewritten in the form

$$\frac{\partial f}{\partial t} + \zeta_j \frac{\partial f}{\partial x_j} = \tilde{Q}[f], \tag{70}$$

where

$$\tilde{Q}[f] = 2J(f_0, f_1) + \epsilon[2J(f_0, f_2) + J(f_1, f_1)] + \epsilon^2 \left[\frac{\partial f_1}{\partial \boldsymbol{h}} \boldsymbol{\Phi}_1 + \frac{\partial f_1}{\partial \nabla \boldsymbol{h}} \nabla \boldsymbol{\Phi}_1 \right]. \tag{71}$$

Since all the coefficients of $\epsilon^k (k = 0, 1, 2)$ in $\tilde{Q}(f)$ are orthogonal to ψ, we can simplify Eq. (69) in the following systematic way. The macroscopic variables $\tilde{\boldsymbol{h}}(x_i, \Delta t)$ are evaluated as

$$\tilde{\boldsymbol{h}}(x_i, \Delta t) = \int_{-\infty}^{\infty} \int_{-\infty}^{\infty} \int_{-\infty}^{\infty} \psi f(x_i - \zeta_i \Delta t, 0, \zeta_i)\, d\zeta_1\, d\zeta_2\, d\zeta_3 - \frac{\Delta t^2}{2} \frac{\partial}{\partial x_i} \times \int_{-\infty}^{\infty} \int_{-\infty}^{\infty} \int_{-\infty}^{\infty} \psi \zeta_i \tilde{Q}(f)(x_i, 0, \zeta_i)\, d\zeta_1\, d\zeta_2\, d\zeta_3 + O(\Delta t^3). \tag{72}$$

If all the terms of $\tilde{Q}[f]$ are omitted, then the error of $\tilde{\boldsymbol{h}}(x_i, \Delta t)$ becomes $O(\Delta t^2)$. This indicates that the intrinsic error of Chou–Baganoff scheme, which is based on the solution of the Cauchy problem for the collisionless equation (66) from the initial data in the form of Eq. (68), is $O(\Delta t^2)$. If $2J(f_0, f_1)$ in $\tilde{Q}[f]$ is retained, which corresponds to Eq. (63), i.e., the exact kinetic equation for the compressible Euler equation, the macroscopic variables are evaluated as

$$\tilde{\boldsymbol{h}}(x_i, \Delta t) = \int_{-\infty}^{\infty} \int_{-\infty}^{\infty} \int_{-\infty}^{\infty} \psi f(x - \zeta_j \Delta t, 0, \zeta_i)\, d\zeta_1\, d\zeta_2\, d\zeta_3 - \Delta t^2 \frac{\partial}{\partial x_j} \times \int_{-\infty}^{\infty} \int_{-\infty}^{\infty} \int_{-\infty}^{\infty} \psi \zeta_j J(f_0, f_1)(x_i, 0, \zeta_i)\, d\zeta_1\, d\zeta_2\, d\zeta_3 + O(\Delta t^3). \tag{73}$$

Comparing Eq. (72) with Eq. (73), we find that the error is $O(\epsilon \Delta t^2)$, which is higher order as long as $\varepsilon \lesssim \Delta t$. In this way, we can control the accuracy of the scheme. Incidentally, the term $J(f_0, f_1)$ in Eq. (63) is independent of the molecular model, and the dependence on the molecular model appears only through f_1 in the initial condition.

One may expect that the replacement of $2J(f_0, f_1)$ in Eq. (63) by the original Boltzmann collision term $(1/\epsilon)J(f, f)$ improves the accuracy. In this case, the macroscopic variables are evaluated as

$$\begin{aligned}\tilde{\boldsymbol{h}}(x_i, \Delta t) &= \int_{-\infty}^{\infty}\int_{-\infty}^{\infty}\int_{-\infty}^{\infty}\psi f(x-\zeta_j\Delta t, 0, \zeta_i)\,d\zeta_1\,d\zeta_2\,d\zeta_3 - \frac{\Delta t^2}{2}\frac{\partial}{\partial x_j}\\ &\quad\times\int_{-\infty}^{\infty}\int_{-\infty}^{\infty}\int_{-\infty}^{\infty}\psi\zeta_j[2J(f_0, f_1)+\epsilon J(f_1, f_1)](x_i, 0, \zeta_i)\,d\zeta_1\,d\zeta_2\,d\zeta_3 + O(\Delta t^3). \quad (74)\end{aligned}$$

Comparing Eq. (72) with Eq. (74), we find that the error is reduced but is still $O(\epsilon\Delta t^2)$.

Finally we consider the kinetic scheme for the Navier–Stokes equation derived from the BGK equation (56). In this case, the basic kinetic equation becomes

$$\frac{\partial f}{\partial t} + \zeta_j\frac{\partial f}{\partial x_j} = \tilde{Q}_{NS\text{–}BGK}[f], \quad (75)$$

where

$$\tilde{Q}_{NS\text{–}BGK}[f] = -\rho(f_1+\epsilon f_2) + \epsilon^2\left[\frac{\partial f_1}{\partial \boldsymbol{h}}\boldsymbol{\Phi}_1 + \frac{\partial f_1}{\partial \nabla\boldsymbol{h}}\nabla\boldsymbol{\Phi}_1\right], \quad (76)$$

and f_1 and f_2 are given by Eqs. (58) and (59), respectively. Since $\tilde{Q}_{NS\text{–}BGK}[f]$ is orthogonal to ψ, the macroscopic variables are evaluated as

$$\begin{aligned}\tilde{\boldsymbol{h}}(x_i, \Delta t) &= \int_{-\infty}^{\infty}\int_{-\infty}^{\infty}\int_{-\infty}^{\infty}\psi f(x-\zeta_j\Delta t, 0, \zeta_i)\,d\zeta_1\,d\zeta_2\,d\zeta_3 + \frac{\Delta t^2}{2}\frac{\partial}{\partial x_j}\\ &\quad\times\int_{-\infty}^{\infty}\int_{-\infty}^{\infty}\int_{-\infty}^{\infty}\psi\zeta_j\tilde{Q}_{NS\text{–}BGK}[f](x_i, 0, \zeta_i)\,d\zeta_1\,d\zeta_2\,d\zeta_3 + O(\Delta t^3). \quad (77)\end{aligned}$$

If we employ the simplified kinetic equation

$$\frac{\partial f}{\partial t} + \zeta_j\frac{\partial f}{\partial x_j} = -\rho f_1, \quad (78)$$

which is equivalent to Eq. (63), the error becomes $O(\epsilon\Delta t^2)$ (note that f_1 and f_2 are orthogonal to ψ). Incidentally, the scheme based on Eq. (78) is employed in the numerical demonstration of Ref. [7]. In the same way as in the derivation of Eq. (74), we find that the accuracy is not improved even if the right-hand side of Eq. (78), $-\rho f_1$, is replaced by the original BGK collision term, $\rho(f_0 - f)/\epsilon$. This demonstrates that the intrinsic error of the modified Prendergast–Xu scheme [22], which is based on the Cauchy problem for the BGK equation from the initial condition in the form of Eq. (68), is $O(\epsilon\Delta t^2)$.

3.4. Error of Numerical Flux

In the previous section, we discussed the error of the kinetic scheme for the Navier–Stokes equation at the level of the basic kinetic equation. Here, we discuss the error appearing in the numerical flux.

We consider the spatially one-dimensional case to avoid inessential complexity; hereafter we will omit all the derivatives with respect to x_2 and x_3. Multiplying Eq. (70) by ψ and integrating the result over the whole velocity space R^3, the cell $(s_{j-1/2}, s_{j+1/2})$, and the time interval $(0, \Delta t)$, we have

$$\tilde{\boldsymbol{h}}_j(\Delta t) = \tilde{\boldsymbol{h}}_j(0) - \frac{1}{\Delta x}\left[\boldsymbol{F}\left(x_1 = s_{j+1/2}\right) - \boldsymbol{F}\left(x_1 = s_{j-1/2}\right)\right], \tag{79}$$

where $\tilde{\boldsymbol{h}}_j(t)$ is the average of $\tilde{\boldsymbol{h}}(x_1, t)$ over the cell $(s_{j-1/2}, s_{j+1/2})$, $\Delta x = s_{j+1/2} - s_{j-1/2}$, and $\boldsymbol{F}$ is the numerical flux defined by

$$\boldsymbol{F}(x_1) = \int_0^{\Delta t} \int_{-\infty}^{\infty} \int_{-\infty}^{\infty} \int_{-\infty}^{\infty} \psi \zeta_1 f(x_1, \zeta_i, t)\, d\zeta_1\, d\zeta_2\, d\zeta_3\, dt. \tag{80}$$

In the actual computation of Eq. (80), an approximate solution the Cauchy problem of Eq. (69) from the initial data in the form of Eq. (68) is employed. If the approximate solution of the collisionless Boltzmann equation (66) without the derivative of the Maxwellian, i.e.,

$$f(x_1, \zeta_i, t) = f_0(x_1, 0, \zeta_i) + \epsilon f_1(x_1, 0, \zeta_i), \tag{81}$$

is employed, which corresponds to the Chou–Baganoff scheme, the error of the resulting numerical flux becomes $O(\Delta t^2)$. The approximate solution of the collisionless Boltzmann equation which is correct up to $O(t)$ is

$$f(x_1, \zeta_i, t) = f_0(x_1, 0, \zeta_i) - t\zeta_1 \frac{\partial f_0}{\partial x_1}(x_1, 0, \zeta_i) + \epsilon f_1(x_1, 0, \zeta_i). \tag{82}$$

The error of the resulting numerical flux is, however, still $O(\Delta t^2)$. If the approximate solution

$$f(x_1, \zeta_i, t) = f_0(x_1, 0, \zeta_i) - t\zeta_1 \frac{\partial f_0}{\partial x_1}(x_1, 0, \zeta_i) + \epsilon f_1(x_1, 0, \zeta_i) + 2tJ(f_0, f_1)(x_1, 0, \zeta_i), \tag{83}$$

which is the one for the simplified equation (63), is employed, then the error becomes $O(\epsilon \Delta t^2)$. In the case of the BGK equation, the definition of f_1 changes from Eq. (53) to Eq. (58). The term $2J(f_0, f_1)$, which is independent of the molecular model, is expressed using f_1 for the BGK equation. Then, the approximate solution corresponding to Eq. (83) is

$$f(x_1, \zeta_i, t) = f_0(x_1, 0, \zeta_i) - t\zeta_1 \frac{\partial f_0}{\partial x_1}(x_1, 0, \zeta_i) + \epsilon f_1(x_1, 0, \zeta_i) - t\rho(x_1, 0) f_1(x_1, 0, \zeta_i). \tag{84}$$

The modified Prendergast–Xu scheme for the compressible Navier–Stokes equation [22] is based on the BGK equation (56). In the derivation of the original scheme [13], the initial distribution function is in the form of $f = f_0$. In the modified scheme it is replaced by $f = f_0 + \epsilon f_1$. As shown in Section 3.3, the intrinsic error of the modified scheme

is $O(\epsilon \Delta t^2)$. In the computation of the numerical flux, the discontinuous initial distribution function is considered and the approximate solution with the effect of molecular collisions is employed. The formula of the approximate solution is lengthy and it is difficult to confirm its accuracy. In Ref. [22] Xu applied the same approximation as that employed in the discontinuous case to the case of a smooth initial distribution and obtained Eq. (84). By this coincidence the accuracy of the scheme as well as its legitimacy is confirmed. That is, the modified Prendergast–Xu scheme for the continuous reconstruction with smoothness at the cell boundaries is derived from the BGK equation by the railroad method.

The numerical flux for Eq. (83) or Eq. (84) is expressed in the form

$$\boldsymbol{F} = \Delta t \boldsymbol{F}^{\text{maxwellian}} - \frac{\Delta t^2}{2}(\boldsymbol{F}^{\text{derivative}} - \boldsymbol{F}^{\text{collision}}) + \Delta t \epsilon \boldsymbol{F}^{\text{diffusive}}, \tag{85}$$

where

$$\boldsymbol{F}^{\text{maxwellian}} = \int_{-\infty}^{\infty}\int_{-\infty}^{\infty}\int_{-\infty}^{\infty} \psi \zeta_1 f_0 \, d\zeta_1 \, d\zeta_2 \, d\zeta_3, \tag{86}$$

$$\boldsymbol{F}^{\text{derivative}} = \frac{\partial}{\partial x_1}\int_{-\infty}^{\infty}\int_{-\infty}^{\infty}\int_{-\infty}^{\infty} \psi \zeta_1^2 f_0 \, d\zeta_1 \, d\zeta_2 \, d\zeta_3, \tag{87}$$

$$\begin{aligned}\boldsymbol{F}^{\text{collision}} = \int_{-\infty}^{\infty}\int_{-\infty}^{\infty}\int_{-\infty}^{\infty} \psi \zeta_1 \Bigg[2\left(C_i C_1 - \frac{C^2}{3}\delta_{i1}\right)\frac{\partial u_i}{\partial x_1} \\ + \frac{C_1}{T^{1/2}}\left(C^2 - \frac{5}{2}\right)\frac{\partial T}{\partial x_1}\Bigg] f_0 \, d\zeta_1 \, d\zeta_2 \, d\zeta_3,\end{aligned} \tag{88}$$

$$\boldsymbol{F}^{\text{diffusive}} = \int_{-\infty}^{\infty}\int_{-\infty}^{\infty}\int_{-\infty}^{\infty} \psi \zeta_1 f_1 \, d\zeta_1 \, d\zeta_2 \, d\zeta_3. \tag{89}$$

To demonstrate the role of the collision effect in the same way as in the case of the linear advection equation, we consider the case of continuous reconstruction with smoothness at the cell boundaries. In this case, each part of the numerical flux is expressed as

$$\boldsymbol{F}^{\text{maxwell}} = \begin{pmatrix} \rho u_1 \\ \rho u_1^2 + \frac{1}{2}\rho T \\ \rho u_1 u_2 \\ \rho u_1 u_3 \\ \rho u_1 \left(u_1^2 + u_2^2 + u_3^2 + \frac{5}{2}T\right) \end{pmatrix}, \tag{90}$$

$$\boldsymbol{F}^{\text{derivative}} = \frac{\partial}{\partial x_1}\begin{pmatrix} \rho u_1^2 + \frac{1}{2}\rho T \\ \rho u_1^3 + \frac{3}{2}\rho T u_1 \\ \rho u_1^2 u_2 + \frac{1}{2}\rho T u_2 \\ \rho u_1^2 u_3 + \frac{1}{2}\rho T u_3 \\ \rho\left[u_1^2\left(u_1^2 + u_2^2 + u_3^2 + 4T\right) + \frac{1}{2}T\left(u_2^2 + u_3^2\right) + \frac{5}{4}T^2\right] \end{pmatrix}, \tag{91}$$

$$\boldsymbol{F}^{\text{collision}} = \begin{pmatrix} 0 \\ \frac{2}{3}\rho T \frac{\partial u_1}{\partial x_1} \\ \frac{1}{2}\rho T \frac{\partial u_2}{\partial x_1} \\ \frac{1}{2}\rho T \frac{\partial u_3}{\partial x_1} \\ \rho T\left[\frac{4}{3}u_1 \frac{\partial u_1}{\partial x_1} + u_2 \frac{\partial u_2}{\partial x_1} + u_3 \frac{\partial u_3}{\partial x_1} + \frac{5}{4}\frac{\partial T}{\partial x_1}\right] \end{pmatrix}, \tag{92}$$

$$\boldsymbol{F}^{\text{diffusive}} = \begin{pmatrix} 0 \\ -\frac{2}{3}\gamma_1 T^a \frac{\partial u_1}{\partial x_1} \\ -\frac{1}{2}\gamma_1 T^a \frac{\partial u_2}{\partial x_1} \\ -\frac{1}{2}\gamma_1 T^a \frac{\partial u_3}{\partial x_1} \\ -\frac{4}{3}\gamma_1 T^a u_1 \frac{\partial u_1}{\partial x_1} - \gamma_1 T^a \left(u_2 \frac{\partial u_2}{\partial x_1} + u_3 \frac{\partial u_3}{\partial x_1}\right) - \frac{5}{4}\gamma_2 T^a \frac{\partial T}{\partial x_1} \end{pmatrix}. \tag{93}$$

The numerical flux without $\boldsymbol{F}^{\text{diffusive}}$ constitutes the kinetic scheme for the compressible Euler equation. If $\boldsymbol{F}^{\text{maxwellian}}$, $\boldsymbol{F}^{\text{derivative}}$, and $\boldsymbol{F}^{\text{collision}}$ at the cell boundaries $x_1 = s_{i\pm1/2}$ are computed using the central difference approximation, i.e., Reconstruction-I, the resulting scheme is the Lax–Wendroff scheme. In this reconstruction, the diffusive flux is also computed by the central finite difference approximation. The modified Prendergast–Xu scheme under this reconstruction is the Lax–Wendroff scheme with the central difference approximation of the diffiusive term. The lack of $\boldsymbol{F}^{\text{collision}}$ is equivalent to the creation of a numerical viscosity proportional to Δt, which is easily seen in the case of the BGK equation since $\boldsymbol{F}^{\text{collision}}$ is equal to $-\rho\boldsymbol{F}^{\text{diffusive}}$ (see the last paragraph of Sec. 3.1). Thus, the computation for viscous flows using the kinetic scheme without the collision effect is valid under the condition $\Delta t \ll \epsilon$. Finally, we mention the case of the reconstruction that allows discontinuity at the cell boundaries. In this case, the numerical flux splits into two parts; the formula of the numerical flux is derived by easy but tedious computations and the expression is lengthy. Computer algebra software such as MATHEMATICA is useful for the derivation. For the numerical demonstration of this scheme, we refer the reader to Ref. [7], where the numerical examples are shown for the normal shock problem, for the Cauchy problem without boundary [the initial temperature distribution $T = 1 + \exp(-x_1^2)$ is a misprint of $T = 1 + 2\exp(-x_1^2)$], and for Couette flow between two parallel plates.

ACKNOWLEDGMENTS

The main part of the present study was done while the author was staying at the department of Mathematics, Hong Kong University of Science and Technology. The author expresses his heartfelt thanks to Dr. Kun Xu of the same department for the invitation, many fruitful discussions, and kind hospitality during the stay.

REFERENCES

1. C. Cercignani, R. Illner, and M. Pulvirenti, *The Mathematical Theory of Dilute Gases* (Springer-Verlag, New York, 1994).
2. S. Y. Chou and D. Baganoff, Kinetic flux-vector splitting for the Navier–Stokes equations, *J. Comput. Phys.* **130**, 217 (1997).
3. S. M. Deshpande, *A Second Order Accurate, Kinetic-Theory Based, Method for Inviscid Compressible Flows*, NASA Langley Tech. Paper NO. 2613 (1986).

4. H. Grad, Principles of the kinetic theory of gases, in *Handbuch der physik*, edited by S. Flügge (Springer-Verlag, Berlin, 1958), Vol. XII, pp. 205–294.
5. A. Harten and S. Osher, Uniformly high-order accurate nonoscillatory schemes. I, *SIAM J. Numer. Anal.* **24**, 279 (1987).
6. C. B. Laney, *Computational Gasdynamics* (Cambridge Univ. Press, Cambridge, UK, 1998).
7. T. Ohwada, Boltzmann schemes for the compressible Navier–Stokes equations, in *Rarefied Gas Dynamics* (AIP Conference Proceedings 585), edited by T. J. Bartel and M. Gallis (Am. Insti. of Physics, New York, 2001), pp. 321–328.
8. T. Ohwada, Y. Sone, and K. Aoki, Numerical analysis of the shear and thermal creep flows of a rarefied gas over a plane wall on the basis of the linearized Boltzmann equation. *Phys. Fluids A* **1**, 1588 (1989).
9. T. Ohwada and Y. Sone, Analysis of thermal stress slip flow and negative thermophoresis using the Boltzmann equation for hard-sphere molecules, *Eur. J. Mech. B/Fluids* **11**, 389 (1992).
10. T. Ohwada, Structure of normal shock waves: Direct numerical analysis of the Boltzmann equation for hard-sphere molecules, *Phys. Fluids A* **5**, 217 (1993).
11. C. L. Pekeris and Z. Alterman, Solution of the Boltzmann–Hilbert integral equation II: The coefficients of viscosity and heat conduction, *Proc. Nat. Acad. Sci. U.S.A.* **43**, 998 (1957).
12. B. Perthame, Second-order Boltzmann schemes for compressible Euler equations in one and two space dimensions, *SIAM J. Numer. Anal.* **29**, 1 (1992).
13. K. H. Prendergast and K. Xu, Numerical hydrodynamics from gas-kinetic theory, *J. Comput. Phys.* **109**, 53 (1993).
14. D. I. Pullin, Direct simulation methods for compressible inviscid ideal gas flow, *J. Comput. Phys.* **34**, 231 (1980).
15. Y. Sone, K. Aoki, S. Takata, S. Sugimoto, and A. V. Bobylev, Inappropriateness of the heat-conduction equation for description of a temperature field of a stationary gas in the continuum limit: Examination by asymptotic analysis and numerical computation of the Boltzmann equation, *Phys. Fluids* **8**, 628 (1996).
16. Y. Sone, C. Bardos, F. Golse, and H. Sugimoto, Asymptotic theory of the Boltzmann system, for a steady flow of a slightly rarefied gas with a finite Mach number: General theory, *Eur. J. Mech., B/Fluids* **19**, 325 (2000).
17. Y. Sone, Asymptotic theory of flow of a rarefied gas over a smooth boundary I, in *Rarefied Gas Dynamics*, edited by L. Trilling and H. Y. Wachmann (Academic Press, New York, 1969), pp. 243–253.
18. Y. Sone, Asymptotic theory of flow of a rarefied gas over a smooth boundary II, in *Rarefied Gas Dynamics*, edited by D. Dini (Editrice Tecnico Scientifica, Pisa, 1971), pp. 737–749.
19. Y. Sone, T. Ohwada, and K. Aoki, Temperature jump and Knudsen layer in rarefied gas over a plane wall: Numerical analysis of the linearized Boltzmann equation for hard-sphere molecules, *Phys. Fluids A* **1**, 363 (1989).
20. Y. Sone and K. Aoki, *Molecular Gas Dynamics* (Asakura, Tokyo, 1994) (in Japanese).
21. B. Van Leer, Towards the ultimate conservative difference schemes IV. A new approach to numerical convection, *J. Comput. Phys.* **23**, 276 (1977).
22. K. Xu, A gas-kinetic BGK scheme for the Navier–Stokes equations and its connection with artificial dissipation and Godunov method, *J. Comput. Phys.* **171**, 289 (2001).